Controlling the onset of Hopf bifurcation in the Hodgkin-Huxley model

Yong Xie,[1,2,*] Luonan Chen,[3] Yan Mei Kang,[4] and Kazuyuki Aihara[2]
[1]*MOE Key Laboratory for Strength and Vibration, School of Aerospace, Xi'an Jiaotong University, Xi'an 710049, People's Republic of China*
[2]*Institute of Industrial Science, The University of Tokyo, 4-6-1 Komaba, Meguro-ku, Tokyo 153-8555, Japan*
[3]*Department of Electrical Engineering and Electronics, Osaka Sangyo University, Nakagaito 3-1-1, Daito, Osaka 574-8530, Japan*
[4]*School of Science, Xi'an Jiaotong University, Xi'an 710049, People's Republic of China*
(Received 11 December 2007; revised manuscript received 22 April 2008; published 26 June 2008)

It is a challenging problem to establish safe and simple therapeutic methods for various complicated diseases of the nervous system, particularly dynamical diseases such as epilepsy, Alzheimer's disease, and Parkinson's disease. From the viewpoint of nonlinear dynamical systems, a dynamical disease can be considered to be caused by a bifurcation induced by a change in the values of one or more regulating parameter. Therefore, the theory of bifurcation control may have potential applications in the diagnosis and therapy of dynamical diseases. In this study, we employ a washout filter-aided dynamic feedback controller to control the onset of Hopf bifurcation in the Hodgkin-Huxley (HH) model. Specifically, by the control scheme, we can move the Hopf bifurcation to a desired point irrespective of whether the corresponding steady state is stable or unstable. In other words, we are able to advance or delay the Hopf bifurcation, so as to prevent it from occurring in a certain range of the externally applied current. Moreover, we can control the criticality of the bifurcation and regulate the oscillation amplitude of the bifurcated limit cycle. In the controller, there are only two terms: the linear term and the nonlinear cubic term. We show that while the former determines the location of the Hopf bifurcation, the latter regulates the criticality of the Hopf bifurcation. According to the conditions of the occurrence of Hopf bifurcation and the bifurcation stability coefficient, we can analytically deduce the linear term and the nonlinear cubic term, respectively. In addition, we also show that mixed-mode oscillations (MMOs), featuring slow action potential generation, which are frequently observed in both experiments and models of chemical and biological systems, appear in the controlled HH model. It is well known that slow firing rates in single neuron models could be achieved only by type-I neurons. However, the controlled HH model is still classified as a type-II neuron, as is the original HH model. We explain that the occurrence of MMOs can be related to the presence of the canard explosion where a small oscillation grows through a sequence of canard cycles to a relaxation oscillation as the control parameter moves through an interval of exponentially small width.

DOI: 10.1103/PhysRevE.77.061921 PACS number(s): 87.19.L−, 05.45.−a, 82.40.Bj, 07.05.Dz

I. INTRODUCTION

A dynamical disease is one in which the predominant symptomatology manifests as a disordered interaction between the elements of the organ in question, that is, a systemic breakdown in coordination and control [1–5]. Many neural and mental disorders such as epilepsy, Alzheimer's disease, Parkinson's disease, anxiety, attention deficit hyperactivity disorder (ADHD), and schizophrenia may be interpreted as dynamical diseases [6–8]. Additionally, panting, Cheyne-Stokes breathing, sudden infant death syndrome, and a form of leukemia in which the balance of red and white blood cells, platelets, and lymphocytes is disrupted, can also be considered as dynamical diseases [9]. Within the framework of nonlinear dynamical systems, a dynamical disease can be considered to be caused by a bifurcation induced by a change in the values of one or more regulating parameters, not in an anatomical dysfunction. For example, it is reported that periodic chronic myelogenous leukemia (PCML) can be induced by a Hopf bifurcation [10]. In fact, each of the above-mentioned dynamical diseases can result from some parameter-dependent bifurcation in a corresponding physiological control system. In the case of schizophrenia, the parameter may be the neurotransmitter dopamine (or serotonin or glutamate). With a high level of dopamine transmission, the symptoms of schizophrenia appear, while those of Parkinson's disease appear with rather low levels of the same. On the other hand, a healthy state prevails in the intermediate range [7]. Consequently, finding better treatments to such dynamical diseases requires that we should understand the underlying bifurcation mechanism from the normal state to the pathological one, and avoid the occurrence of bifurcations within a certain range of parameters. In this manner, the theory of bifurcation control may have potential applications in the diagnosis and therapy of dynamical diseases.

Bifurcation control has attracted increasing attention and become an ongoing active and fruitful area of research. Bifurcation control deals with modification of bifurcation characteristics of a parametrized nonlinear system by a designed control input, so as to obtain some desired dynamical behavior or to avoid undesirable instability around bifurcations. The goals of bifurcation control include delaying the onset of an inherent bifurcation, modifying the shape or type of a bifurcation chain, introducing a new bifurcation at a preferable parameter value, stabilizing a bifurcated solution or

*yxie@mail.xjtu.edu.cn

branch, changing the parameter value of an existing bifurcation point, monitoring the multiplicity, amplitude, and/or frequency of some limit cycles emerging from bifurcations, optimizing the system performance near a bifurcation point, or a certain combination of some of these [11]. Currently, representative approaches of bifurcation control include washout filter-aided dynamic feedback [12], linear or nonlinear state feedback [13,14], harmonic balance approximation [15], and quadratic invariants in normal forms [16]. Bifurcation control has been employed to eliminate seizing behavior in the model system of human cortical electrical activity [17], and to stabilize high angle-of-attack flight dynamics [18].

In this study, we focus our attention on controlling the onset of bifurcations in an individual neuron via bifurcation control. In our previous paper [19], we applied the bifurcation control to a simple two-dimensional Hindmarsh-Rose type neuron model [20] to change the types of neuronal excitability. As is well known, the Hodgkin-Huxley (HH) model [21] is a paradigmatic model of neurons, and it undergoes a Hopf bifurcation from the steady state to periodic spiking when the externally applied current is regarded as a bifurcation parameter. Therefore, we take the HH model as an example to show our control scheme and results with a more realistic neuron model. In the HH model, we aim to advance or delay the Hopf bifurcation to avoid its occurrence in a certain range of externally applied current by using a washout filter-aided dynamic feedback controller. Although the bifurcation control of the HH model has already been studied [22], there are no clear mathematical criteria to select the control gains. In this paper, according to the two basic critical conditions for the emergence of the Hopf bifurcation, i.e., the eigenvalue assignment and the transversality condition [23,24], we employ an effective criterion to analytically determine the control gains and move the Hopf bifurcation to a desired parameter value. By the application of the center manifold and normal form theory, we derive a closed-form analytical expression for the bifurcation stability coefficient, which dominates the criticality of the Hopf bifurcation and simultaneously regulates the oscillation amplitude. In addition, we show the mixed-mode oscillation (MMO) pattern and describe its dynamical mechanism.

This paper is organized as follows. In Sec. II, we briefly describe the HH model and show its bifurcation behavior with variation in the externally applied current. In Sec. III, we employ a washout filter-aided dynamic feedback controller to advance the Hopf bifurcation toward a stable equilibrium point where the criticality of the bifurcation is also transformed from subcritical to supercritical. Simultaneously, we show that the MMO patterns occur in the controlled HH model. Moreover, the oscillation amplitude of the bifurcated periodic solution is also controlled simultaneously. In Sec. IV, we delay the Hopf bifurcation until an unstable equilibrium point. In Sec. V, we present the conclusions by giving several general remarks.

II. HODGKIN-HUXLEY MODEL AND ITS BIFURCATION DYNAMICS

The HH model is a quantitative model that describes how the action potentials in neurons are initiated and propagated. It is a set of nonlinear ordinary differential equations that approximates the electrical characteristics of the nerve membrane [21]. The HH equations are given as follows:

$$\frac{dV}{dt} = \frac{1}{C_M}[I_{\text{ext}} - g_{\text{Na}}m^3h(V - V_{\text{Na}}) - g_{\text{K}}n^4(V - V_K) - g_L(V - V_L)],$$

$$\frac{dm}{dt} = \alpha_m(V)(1 - m) - \beta_m(V)m,$$

$$\frac{dh}{dt} = \alpha_h(V)(1 - h) - \beta_h(V)h,$$

$$\frac{dn}{dt} = \alpha_n(V)(1 - n) - \beta_n(V)n.$$

V represents the membrane potential, which is the electrical potential difference (voltage) across the nerve membrane. m and h are gating variables that represent the activation and inactivation of the sodium ion channel, respectively. n denotes the activation gating variable of the potassium ion channel. Obviously, m, h, and n obey equations of the same form, but with different voltage dependences for their steady-state values and time constants. α_m, β_m, α_h, β_h, α_n, and β_n are functions of V that are defined as follows:

$$\alpha_m(V) = 0.1(25.0 - V)/\{\exp[(25.0 - V)/10.0] - 1.0\},$$

$$\beta_m(V) = 4.0\exp(-V/18.0),$$

$$\alpha_h(V) = 0.07\exp(-V/20.0),$$

$$\beta_h(V) = 1.0/\{\exp[(-V + 30.0)/10.0] + 1.0\},$$

$$\alpha_n(V) = 0.01(10.0 - V)/\{\exp[(10.0 - V)/10.0] - 1.0\},$$

$$\beta_n(n) = 0.125\exp(-V/80.0).$$

The HH model includes the following parameters: $V_{\text{Na}} = 115.0$ mV, $V_{\text{K}} = -12.0$ mV, and $V_L = 10.599$ mV, respectively, representing the equilibrium potentials of the sodium, potassium, and leak currents, and are determined by the Nernst equation. Thus, these parameter values are controllable by changing the ionic concentrations inside and outside the membrane. $g_{\text{Na}} = 120.0$ mS/cm^2, $g_{\text{K}} = 36.0$ mS/cm^2, and $g_L = 0.3$ mS/cm^2 represent the maximum conductance of the corresponding ionic currents, which reflect the ionic-channel density distributed over the membrane. $C_M = 1.0$ μF/cm^2 is the membrane capacitance. I_{ext} represents the externally applied current, and in this study, we consider it to be a time-independent dc current that serves as a bifurcation parameter of the system.

The bifurcation diagram for the membrane potential V as a function of I_{ext} is shown in Fig. 1. From Fig. 1(a), we can see that the neuron undergoes a Hopf bifurcation (HB) from quiescence to periodic spiking at $I_{\text{ext}} = 9.780$ μA/cm^2. Moreover, the amplitude of the stable periodic oscillation de-

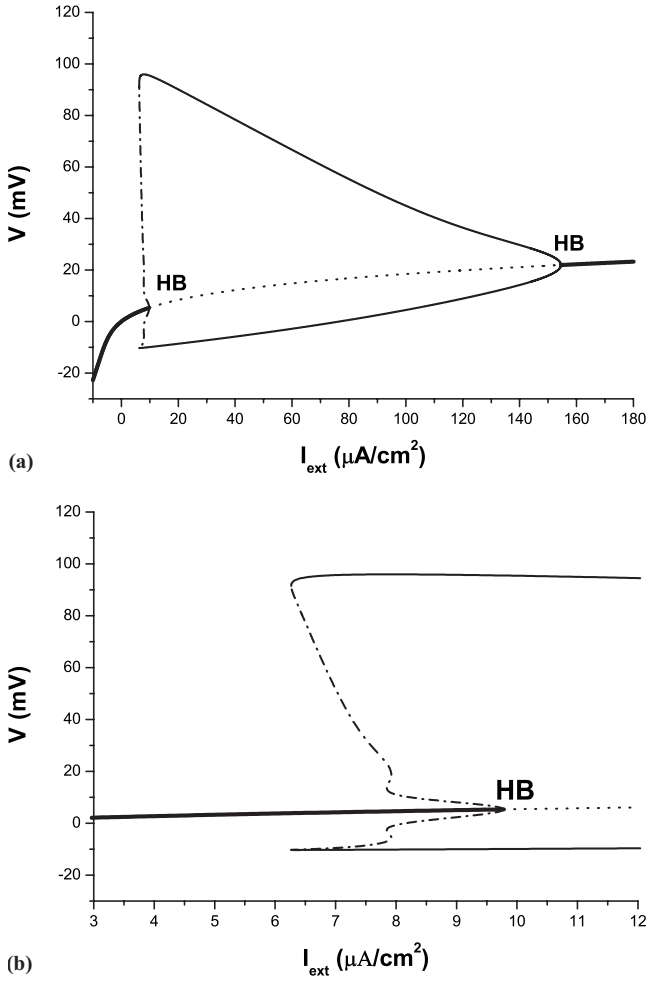

FIG. 1. (a) Bifurcation diagram of the HH model. The thick solid lines represent stable equilibrium points, while the dotted line represents unstable ones. The maxima and minima of stable and unstable limit cycles are indicated by thin and dashed lines, respectively. (b) The enlargement of (a) near the left Hopf bifurcation point. The lines of all other bifurcation diagrams in this paper are the same as this caption.

creases with an increase in the externally applied current, and the periodic oscillation terminates at $I_{\text{ext}}=154.527\ \mu\text{A}/\text{cm}^2$, where another Hopf bifurcation occurs. From Fig. 1(b), it can be seen that the left Hopf bifurcation is subcritical. Henceforth, we will restrict our discussions to the left Hopf bifurcation because it is related to the dynamical mechanism of neuronal excitability from quiescence to firing [25], in contrast to the right Hopf bifurcation, where the intensity of the external stimulus current generally exceeds the normal physiological range.

Note that all bifurcation diagrams in this paper were produced using the software package XPPAUT [26], which is software for the analysis and simulation of dynamical systems and can detect several bifurcation points automatically and can trace both stable and unstable branches of steady states and periodic solutions. In the XPPAUT software package, the fundamental tool of AUTO interface is pseudoarclength continuation, which is the most popular numerical continuation method [27]. As we know, the ideal parametrization of a curve is arclength, and pseudoarclength is an approximation of the arclength in the tangent space of the curve. Geometrically interpreted, the algorithm of pseudoarclength continuation finds a solution to the nonlinear system in a hyperplane that is at a distance of pseudoarclength Δs from the current solution and that is perpendicular to the tangent vector of the current solution. Usually a predictor-corrector method is applied to find the solution at the given pseudoarclength Δs [27].

III. BIFURCATION ADVANCE TOWARD $I_{\text{ext}}=5.0\ \mu\text{A}/\text{cm}^2$

In this section, we first employ a washout filter-aided dynamic feedback controller to advance the Hopf bifurcation toward $I_{\text{ext}}=5.0\ \mu\text{A}/\text{cm}^2$, derive the conditions to transform the criticality of the bifurcation from subcritical into supercritical, display the occurrence of the MMO pattern in the controlled HH model, and finally show the regulation of the oscillation amplitude.

A. Bifurcation advance

We advance the Hopf bifurcation point by a washout filter-aided dynamic feedback controller. Actually, a washout filter is a high-pass filter that washes out steady-state inputs while passing transient inputs [28]. The use of washout filters ensures that all the equilibrium points of the original system are preserved in the controlled system, i.e., their location remains unchanged. Recently, it was reported that washout filter-aided dynamic feedback controllers can be employed for the creation of Hopf bifurcations in continuous-time systems with arbitrary dimensions [29]. Here, we only add one washout filter-aided dynamic feedback controller to the right-hand side of the equation of the membrane potential. In this study, we select the membrane voltage as an input to the washout filter because it can be readily measured, and the controller can be realized easily. Therefore, the equation of the membrane potential with a washout filter-aided dynamic feedback controller can be written as follows:

$$\frac{dV}{dt}=\frac{1}{C_M}[I_{\text{ext}}-g_{\text{Na}}m^3h(V-V_{\text{Na}})-g_{\text{K}}n^4(V-V_{\text{K}})-g_L(V-V_L)+u],$$

where u denotes the control input. On the other hand, the equations for m, h, and n are the same as the HH model.

The washout filter-aided dynamic feedback controller assumes the following dynamics [24]:

$$\frac{dw}{dt}=V-dw\triangleq y,$$

$$u=g(y),$$

where w and y are the state variable and the output variable of the washout filter, respectively. g denotes the nonlinear control function to be designed, and d denotes the reciprocal of the filter time constant. As a result, the controlled system is not four-dimensional but five-dimensional. There are two constraint conditions that should be satisfied: one is $d>0$,

which guarantees the stability of the washout filter; the other is $g(0)=0$, which preserves the original equilibrium points. Due to the nature of the washout filter, $u=0$ for $\dot{w}=y=0$. Hence, all the equilibrium points remain unchanged when control actions are applied. In this paper, we set $d=0.1$.

It is well known that only the quadratic and cubic terms in a nonlinear system undergoing a Hopf bifurcation influence the stability of the bifurcation [13,14]. However, in order to simplify the selection of control parameters, we adopt a controller having the following simple form with only a linear term and a cubic term:

$$u = K_l(V - dw) + K_n(V - dw)^3.$$

In what follows, we first determine the linear control gain K_l because in our controller it only can contribute to the location of the bifurcation point and advance the bifurcation toward $I_{\text{ext}}=5.0\ \mu\text{A/cm}^2$.

At $I_{\text{ext}}=5.0\ \mu\text{A/cm}^2$, the original HH model behaves as a single stable steady state, i.e., the stable equilibrium point $(V_0,m_0,h_0,n_0)=(3.266\,72,0.077\,20,0.479\,38,0.368\,70)$. However, the controlled HH has a modified equilibrium point at $I_{\text{ext}}=5.0\ \mu\text{A/cm}^2$, namely, $(V_0,m_0,h_0,n_0,w_0)=(V_0,m_0,h_0,n_0,V_0/d)$, from which a Hopf bifurcation emanates. At this point, we can calculate the Jacobian matrix of the controlled system. The characteristic equation of the Jacobian matrix has the following form:

$$p_0\lambda^5 + p_1\lambda^4 + p_2\lambda^3 + p_3\lambda^2 + p_4\lambda + p_5 = 0,$$

where p_j with $j=0,1,\ldots,5$ are dependent on the system parameters, the location of the equilibrium point, and the linear control gain. Substituting them into p_j, we can obtain

$$p_0 = 1.0,$$

$$p_1 = 5.021\,04 - K_l,$$

$$p_2 = 2.285\,53 - 3.929\,30K_l,$$

$$p_3 = 1.621\,61 - 1.159\,11K_l,$$

$$p_4 = 0.310\,98 - 0.085\,22K_l,$$

$$p_5 = 0.016\,68.$$

It is well known that if a Hopf bifurcation occurs at $I_{\text{ext}}=5.0\ \mu\text{A/cm}^2$, the Jacobian matrix of the controlled system must satisfy two basic critical conditions, i.e., the eigenvalue crossing condition and the transversality condition. One type of degenerate Hopf bifurcation is the failure of the transversality condition. Therefore, the characteristic equation has a pair of pure imaginary eigenvalues $\lambda_1=\omega_0 i$ and $\lambda_2=\bar{\lambda}_1=-\omega_0 i$, and the remaining eigenvalues have negative real parts. Here, i is the imaginary unit. At the same time, the eigenvalues λ_1 and λ_2 cross the imaginary axis at some nonzero speed at the bifurcation point. In order to avoid directly solving all eigenvalues, we adopt an effective criterion for detecting the existence of Hopf bifurcations, which is based on the Routh-Hurwitz stability criterion and is described by p_j instead of the eigenvalues [30].

Thus, the eigenvalue crossing condition is equivalent to the following conditions:

$$p_5 > 0,$$

$$\Delta_j > 0, \quad j = 1,2,3,$$

$$\Delta_4 = 0,$$

where

$$\Delta_1 = p_1,$$

$$\Delta_2 = \begin{vmatrix} p_1 & p_0 \\ p_3 & p_2 \end{vmatrix},$$

$$\Delta_3 = \begin{vmatrix} p_1 & p_0 & 0 \\ p_3 & p_2 & p_1 \\ p_5 & p_4 & p_3 \end{vmatrix},$$

$$\Delta_4 = \begin{vmatrix} p_1 & p_0 & 0 & 0 \\ p_3 & p_2 & p_1 & p_0 \\ p_5 & p_4 & p_3 & p_2 \\ 0 & 0 & p_5 & p_4 \end{vmatrix}.$$

On the other hand, the transversality condition is expressed by

$$\frac{d(\Delta_4)}{dI_{\text{ext}}} \neq 0.$$

Substituting p_i, $i=0,1,\ldots,5$, into the eigenvalue crossing condition, we obtain

$$\Delta_1 = 5.021\,04 - K_l > 0,$$

$$\Delta_2 = 3.929\,30K_l^2 - 20.855\,62K_l + 9.854\,13 > 0,$$

$$\Delta_3 = -4.469\,26K_l^3 + 29.378\,90K_l^2 - 39.987\,01K_l + 8.223\,24 > 0,$$

$$\Delta_4 = 0.380\,88K_l^4 - 3.636\,14K_l^3 + 11.029\,23K_l^2 - 11.707\,80K_l + 2.207\,47 = 0.$$

Obviously, $p_5>0$ holds.

Solving the above inequalities and the equation, we can obtain

$$K_l = 0.237\,71.$$

With regard to the transversality condition, it can be numerically computed as

$$\frac{d(\Delta_4)}{dI_{\text{ext}}} = -0.325 \neq 0,$$

which satisfies the transversality condition.

In this manner, we make the Hopf bifurcation at $I_{\text{ext}}=9.780\ \mu\text{A/cm}^2$ advance toward $I_{\text{ext}}=5.0\ \mu\text{A/cm}^2$, which is

clearly not degenerate in the sense of the transversality.

From the above calculation, it can be seen that K_n has no effect on the location of the bifurcation point. Therefore, we temporarily assume $K_n=0$, and calculate the bifurcation diagram of the controlled system, as shown in Fig. 2. As expected, the Hopf bifurcation has been successfully advanced toward $I_{\text{ext}}=5.0\ \mu\text{A}/\text{cm}^2$, and is still subcritical.

B. Controlling the criticality of Hopf bifurcation

In this subsection, we control the criticality of the advanced Hopf bifurcation by the nonlinear control gain K_n. Whether a Hopf bifurcation is subcritical or supercritical is determined typically by the sign of the bifurcation stability coefficient of the dynamical system near the equilibrium. The bifurcated limit cycle is orbitally stable or the bifurcation is supercritical if the bifurcation stability coefficient is negative. Otherwise, it is unstable and the bifurcation is subcritical.

In what follows, we apply the center manifold and normal form theory to derive the closed-form analytical expression of the bifurcation stability coefficient β_2 for the controlled HH model. After determining the linear control gain, $K_l=0.237\,71$, the Jacobian matrix of the controlled system becomes a constant matrix. In this manner, we can numerically calculate all eigenvalues of the matrix and their corresponding eigenvectors. Actually, this is a necessary step in deriving β_2 with respect to K_n in order to employ the center manifold and normal form theory.

The constant matrix is given as

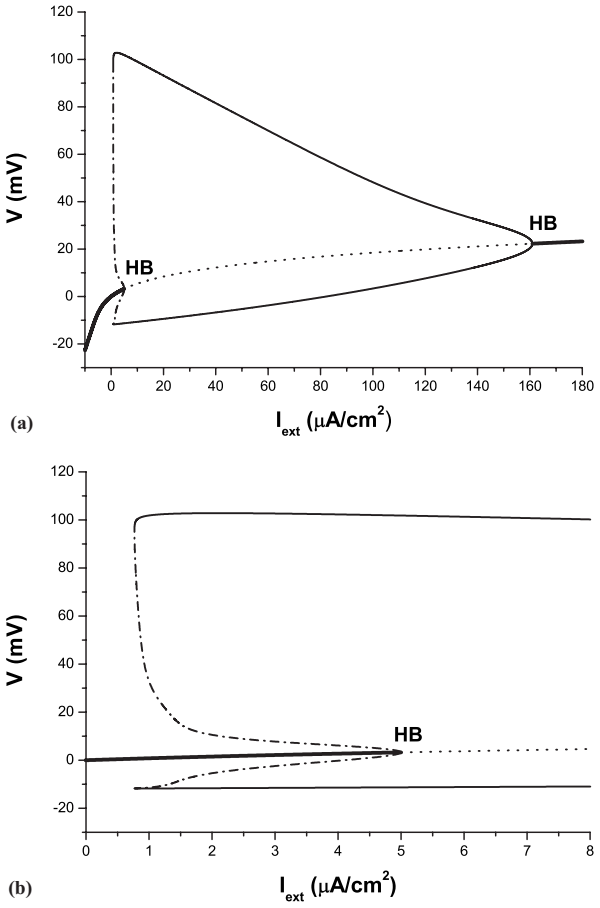

FIG. 2. (a) Bifurcation diagram of the controlled HH model with $K_l=0.237\,71$ and $K_n=0$. (b) The enlargement of (a) near the left Hopf bifurcation point.

$$\begin{bmatrix} -0.754\,03 & 114.909\,65 & 6.168\,08 & -110.187\,29 & -0.023\,77 \\ 0.031\,52 & -3.615\,20 & 0.0 & 0.0 & 0.0 \\ -0.0044 & 0.0 & -0.124\,02 & 0.0 & 0.0 \\ 0.003\,01 & 0.0 & 0.0 & -0.190\,08 & 0.0 \\ 1.0 & 0.0 & 0.0 & 0.0 & -0.1 \end{bmatrix}.$$

The eigenvalues and their corresponding eigenvectors are as follows:

$$\lambda_1 = 7.564\,28 \times 10^{-19} + 0.518\,10i,$$

$$\lambda_2 = 7.564\,28 \times 10^{-19} - 0.518\,10i,$$

$$\lambda_3 = -0.104\,82,$$

$$\lambda_4 = -0.130\,31,$$

$$\lambda_5 = -4.548\,20,$$

and

$$v_1 = \begin{bmatrix} -0.088\,44 - 0.458\,21i \\ -0.001\,32 - 0.003\,81i \\ 0.003\,89 + 0.000\,17i \\ -0.002\,51 - 0.000\,41i \\ -0.884\,41 \end{bmatrix}, \quad v_2 = \bar{v}_1,$$

$$v_3 = \begin{bmatrix} 0.004\,82 \\ 0.000\,04 \\ -0.001\,11 \\ 0.000\,17 \\ -1.000\,00 \end{bmatrix}, \quad v_4 = \begin{bmatrix} 0.030\,29 \\ 0.000\,27 \\ 0.021\,38 \\ 0.001\,53 \\ -0.999\,31 \end{bmatrix},$$

$$v_5 = \begin{bmatrix} 0.975\,12 \\ -0.032\,94 \\ 0.000\,98 \\ -0.000\,67 \\ -0.219\,22 \end{bmatrix}.$$

Due to the very small real parts of λ_1 and λ_2, the matrix can be approximately considered to have a pair of pure imaginary eigenvalues. The remaining eigenvalues are negative. For notational simplicity, let $\omega_0 = 0.518\,10$ and

$$M = \begin{bmatrix} -0.104\,82 & 0 & 0 \\ 0 & -0.130\,31 & 0 \\ 0 & 0 & -4.548\,20 \end{bmatrix}.$$

We construct a matrix in the following manner:

$$P = (\mathrm{Re}(v_1), -\mathrm{Im}(v_1), v_3, v_4, v_5)$$

and take the following coordinate transformation:

$$\begin{bmatrix} V \\ m \\ h \\ n \\ w \end{bmatrix} = \begin{bmatrix} V_0 \\ m_0 \\ h_0 \\ n_0 \\ w_0 \end{bmatrix} + P \begin{bmatrix} X_1 \\ X_2 \\ X_3 \\ X_4 \\ X_5 \end{bmatrix}.$$

Substituting the coordinate transformation into the controlled HH model, and then making the following transformation, we can obtain a system under a new coordinate system as follows:

$$\begin{bmatrix} \frac{dX_1}{dt} \\ \frac{dX_2}{dt} \\ \frac{dX_3}{dt} \\ \frac{dX_4}{dt} \\ \frac{dX_5}{dt} \end{bmatrix} = P^{-1} \begin{bmatrix} \frac{dV}{dt} \\ \frac{dm}{dt} \\ \frac{dh}{dt} \\ \frac{dn}{dt} \\ \frac{dw}{dt} \end{bmatrix} = \begin{bmatrix} F^1(X_1,X_2,X_3,X_4,X_5) \\ F^2(X_1,X_2,X_3,X_4,X_5) \\ F^3(X_1,X_2,X_3,X_4,X_5) \\ F^4(X_1,X_2,X_3,X_4,X_5) \\ F^5(X_1,X_2,X_3,X_4,X_5) \end{bmatrix},$$

where P^{-1} is the inverse matrix of P, and

$$P^{-1} = \begin{bmatrix} 0.201\,96 & 14.330\,78 & 20.828\,77 & -351.562\,57 & -0.081\,41 \\ 1.801\,44 & 55.205\,35 & 2.581\,42 & -86.031\,12 & -0.006\,45 \\ -0.181\,56 & -5.943\,16 & -58.321\,20 & 234.621\,91 & -0.896\,26 \\ -0.040\,82 & -1.345\,96 & 39.987\,79 & 75.253\,03 & -0.032\,01 \\ 0.199\,50 & -24.570\,17 & -0.278\,13 & 5.043\,88 & 0.001\,07 \end{bmatrix}.$$

At $(X_1,X_2,X_3,X_4,X_5)=(0,0,0,0,0)$, by ignoring very small entries, the Jacobian matrix of the new system has the real canonical form

$$\begin{bmatrix} 0 & -\omega_0 & 0 \\ \omega_0 & 0 & 0 \\ 0 & 0 & M \end{bmatrix}.$$

In this manner, we can employ the center manifold and normal form theory to derive the closed-form analytical expression for the bifurcation stability coefficient β_2, which has a unified expression for a system possessing a real canonical form by following the same procedures in [31]. Therefore, we can take advantage of the expression of the bifurcation stability coefficient β_2 in a straightforward way, which is written as

$$\beta_2(K_n) = 2\,\mathrm{Re}\left[\left(g_{20}g_{11} - 2|g_{11}|^2 - \tfrac{1}{3}|g_{02}|^2\right)\frac{i}{2\omega_0} + \frac{g_{21}(K_n)}{2}\right],$$

where

$$g_{20} = \frac{1}{4}\left[\frac{\partial^2 F^1}{\partial X_1^2} - \frac{\partial^2 F^1}{\partial X_2^2} + 2\frac{\partial^2 F^2}{\partial X_1 \partial X_2} + i\left(\frac{\partial^2 F^2}{\partial X_1^2} - \frac{\partial^2 F^2}{\partial X_2^2} - 2\frac{\partial^2 F^1}{\partial X_1 \partial X_2}\right)\right],$$

$$g_{11} = \frac{1}{4}\left[\frac{\partial^2 F^1}{\partial X_1^2} + \frac{\partial^2 F^1}{\partial X_2^2} + i\left(\frac{\partial^2 F^2}{\partial X_1^2} + \frac{\partial^2 F^2}{\partial X_2^2}\right)\right],$$

$$g_{02} = \frac{1}{4}\left[\frac{\partial^2 F^1}{\partial X_1^2} - \frac{\partial^2 F^1}{\partial X_2^2} - 2\frac{\partial^2 F^2}{\partial X_1 \partial X_2} + i\left(\frac{\partial^2 F^2}{\partial X_1^2} - \frac{\partial^2 F^2}{\partial X_2^2} + 2\frac{\partial^2 F^1}{\partial X_1 \partial X_2}\right)\right],$$

$$g_{21}(K_n) = G_{21}(K_n) + \sum_{k=1}^{3}(2G_{110}^k s_{11}^k + G_{101}^k s_{20}^k),$$

$$G_{21}(K_n) = \frac{1}{8}\left[\frac{\partial^3 F^1}{\partial X_1^3} + \frac{\partial^3 F^1}{\partial X_1 \partial X_2^2} + \frac{\partial^3 F^2}{\partial X_1^2 \partial X_2} + \frac{\partial^3 F^2}{\partial X_2^3} + i\left(\frac{\partial^3 F^2}{\partial X_1^3} + \frac{\partial^3 F^2}{\partial X_1 \partial X_2^2} - \frac{\partial^3 F^1}{\partial X_1^2 \partial X_2} - \frac{\partial^3 F^1}{\partial X_2^3}\right)\right]$$

$$G_{110}^{j-2} = \frac{1}{2}\left[\frac{\partial^2 F^1}{\partial X_1 \partial X_j} + \frac{\partial^2 F^2}{\partial X_2 \partial X_j} + i\left(\frac{\partial^2 F^2}{\partial X_1 \partial X_j} - \frac{\partial^2 F^1}{\partial X_2 \partial X_j}\right)\right],$$

$$G_{101}^{j-2} = \frac{1}{2}\left[\frac{\partial^2 F^1}{\partial X_1 \partial X_j} - \frac{\partial^2 F^2}{\partial X_2 \partial X_j} + i\left(\frac{\partial^2 F^1}{\partial X_2 \partial X_j} + \frac{\partial^2 F^2}{\partial X_1 \partial X_j}\right)\right]$$

for $j=3,4,5$.

s_{11}^k and s_{20}^k are the components of the three-dimensional vectors $s_{11}=(s_{11}^1,s_{11}^2,s_{11}^3)^T$ and $s_{20}=(s_{20}^1,s_{20}^2,s_{20}^3)^T$, respectively. Here, the vectors s_{11} and s_{20} are the solutions of the following linear equations, respectively:

$$Ms_{11} = -h_{11} \text{ and } (M - 2i\omega_0 I)s_{20} = -h_{20},$$

where I represents the 3×3 identity matrix. $h_{11}=(h_{11}^1,h_{11}^2,h_{11}^3)^T$ and $h_{20}=(h_{20}^1,h_{20}^2,h_{20}^3)^T$ are three-dimensional vectors with the following components:

$$h_{11}^{j-2} = \frac{1}{4}\left(\frac{\partial^2 F^j}{\partial X_1^2} + \frac{\partial^2 F^j}{\partial X_2^2}\right),$$

$$h_{20}^{j-2} = \frac{1}{4}\left(\frac{\partial^2 F^j}{\partial X_1^2} - \frac{\partial^2 F^j}{\partial X_2^2} - 2i\frac{\partial^2 F^j}{\partial X_1 \partial X_2}\right)$$

for $j=3,4,5$.

Note that the expressions of g_{20}, g_{11}, and g_{02} are not changed for a system of arbitrary dimension with a real canonical form in the expression of β_2, and they are just subjected to the former two equations. On the other hand, all the equations of the system contribute to the expression of $g_{21}(K_n)$.

As given above, all derivatives take values at $(X_1,X_2,X_3,X_4,X_5)=(0,0,0,0,0)$. Consequently, we can obtain the closed-form analytical expression for β_2 as follows:

$$\beta_2 = 0.987\,84 \times 10^{-3} + 2\,\mathrm{Re}(-i0.728\,60 \times 10^{-2}K_n + 0.649\,90 \times 10^{-1}K_n).$$

If K_n is a real number with $K_n<-7.5999\times 10^{-3}$, $\beta_2<0$. Thus, $K_n<-7.5999\times 10^{-3}$ ensures that the limit cycle bifurcated from the Hopf bifurcation is asymptotically stable, and that the Hopf bifurcation is supercritical. In contrast, if $K_n>-7.5999\times 10^{-3}$, $\beta_2>0$ and the bifurcation is subcritical. In order to confirm the accuracy of our analytical expression for β_2, we calculate the bifurcation diagrams of the controlled system for the two cases of $K_n<-7.5999\times 10^{-3}$ and $K_n>-7.5999\times 10^{-3}$. Let $K_n=-0.008$ and -0.007, respectively. When $K_n=-0.008$, the corresponding bifurcation diagram is shown in Fig. 3. From Fig. 3(b), it is evident that the Hopf bifurcation is supercritical. Figure 4 shows the bifurcation diagram of the controlled system with $K_n=-0.007$. Obviously, the Hopf bifurcation of Fig. 4(b) is subcritical. Figures 3 and 4 confirm the validity of the criterion and the expression for the bifurcation stability coefficient. At the same time, we can see that the location of the bifurcation point remains unchanged, i.e., it remains at $I_{\text{ext}}=5.0\ \mu\text{A/cm}^2$. This shows that K_n does not contribute to the location of the bifurcation point, but it can influence the criticality of the bifurcation.

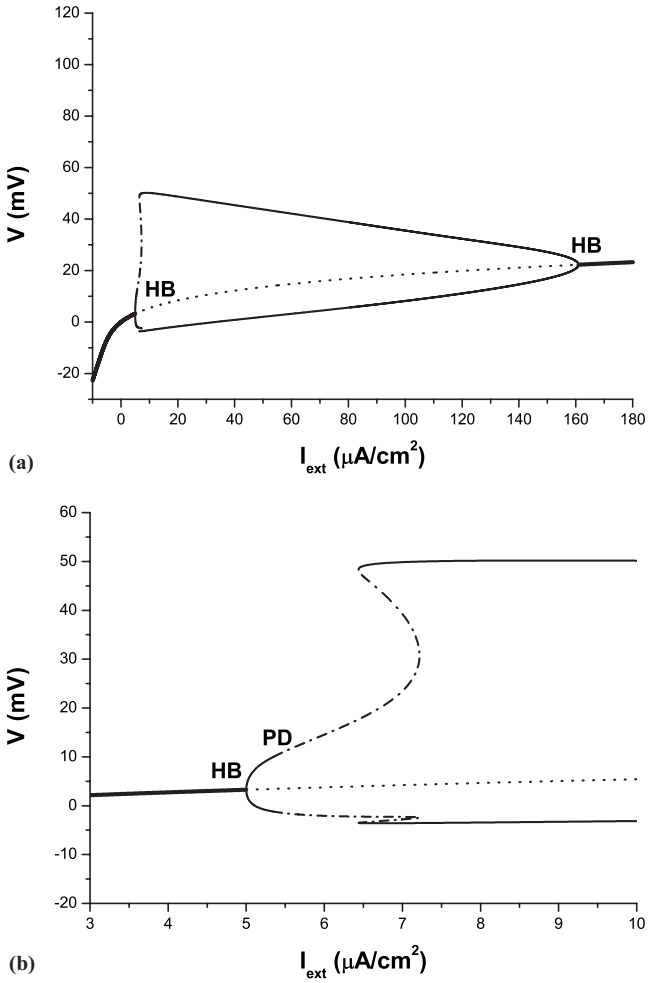

FIG. 3. (a) Bifurcation diagram of the controlled HH model with $K_l=0.237\,71$ and $K_n=-0.008$. (b) The enlargement of (a) near the left Hopf bifurcation point.

C. Mixed-mode oscillations

We can see that there are period-doubling (PD) cascades in Figs. 3(b) and 4(b) that closely follow the Hopf bifurcations where we simply mark the locations of the first period-doubling bifurcations, and those of the second and higher ones are not shown. For example, let us investigate the neuronal behavior in the range of I_{ext} from 5.2 to 6.5 $\mu\text{A/cm}^2$ under the condition of $K_l=0.237\,71$ and $K_n=-0.008$ in a different method. That is, we study the change in local maxima of the membrane potential as a function of I_{ext}, which can be considered as a form of Poincaré section, as shown in Fig. 5. Evidently, neuronal oscillations exhibit the alternating chaotic and periodic responses as I_{ext} is varied. From Fig. 5(b), we can see that a series of period-doubling bifurcations leads from periodic oscillations to chaotic ones, which is a classical road to chaos in dynamical systems.

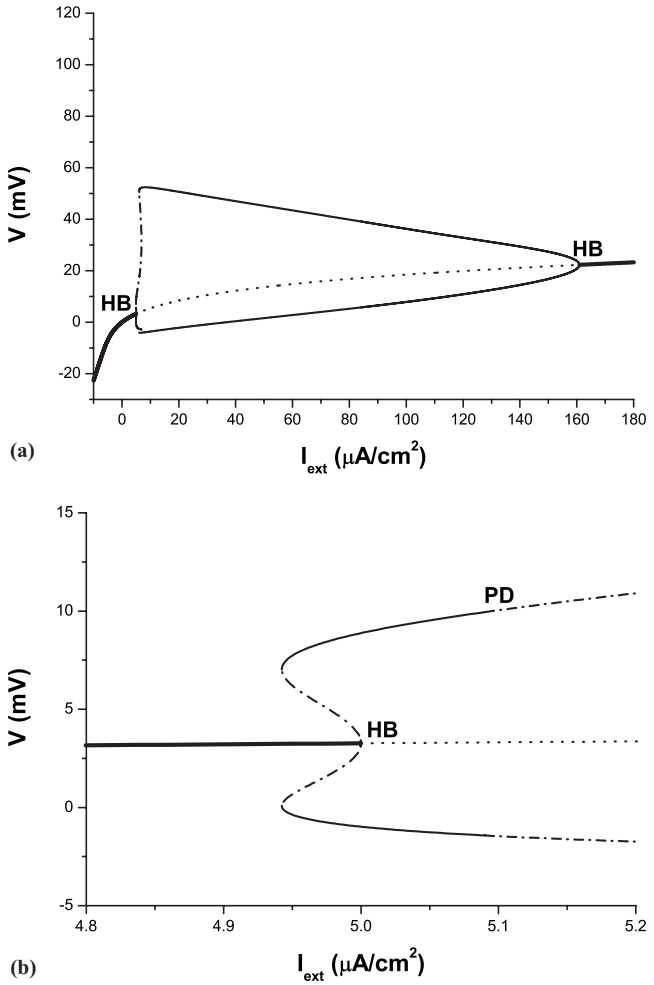

FIG. 4. (a) Bifurcation diagram of the controlled HH model with K_l=0.237 71 and K_n=−0.007. (b) The enlargement of (a) near the left Hopf bifurcation point.

Figure 6 shows the time series of the membrane potential at I_{ext}=5.5 μA/cm^2. This periodic spiking is a famous mixed-mode oscillation (MMO), which is a phenomenon quite often encountered in both experiments and models of chemical and biological systems [32,33]. In general, MMOs consist of L large-amplitude relaxation oscillations followed by s small-amplitude oscillations, and the symbol L^s is assigned to this pattern [34]. In the context of neurodynamics, large-amplitude relaxation oscillations correspond to firing of action potentials while small-amplitude oscillations correspond to subthreshold oscillations (STOs). In this paper, L denotes the number of large peaks and s is the number of small peaks in one period. For example, the time series of the membrane potential in Fig. 6 is a 1^3 mixed-mode oscillation. According to Fig. 5(a), we can determine that I_{ext}=5.7, 6.0, 6.2, and 6.33 μA/cm^2 correspond to 1^2, 1^1, 2^1, and 3^1 MMOs, respectively. Figure 7 shows the time series of the membrane potential when I_{ext}=6.33 μA/cm^2, and it displays clearly a 3^1 MMO. In Fig. 5, the regions in which the profile of lines is clear correspond to periodic oscillations, such as I_{ext}=5.5 and 6.33 μA/cm^2, which are shown in Figs. 6 and 7, respectively. On the other hand, the regions where the profile of lines is vague correspond to chaotic oscillations.

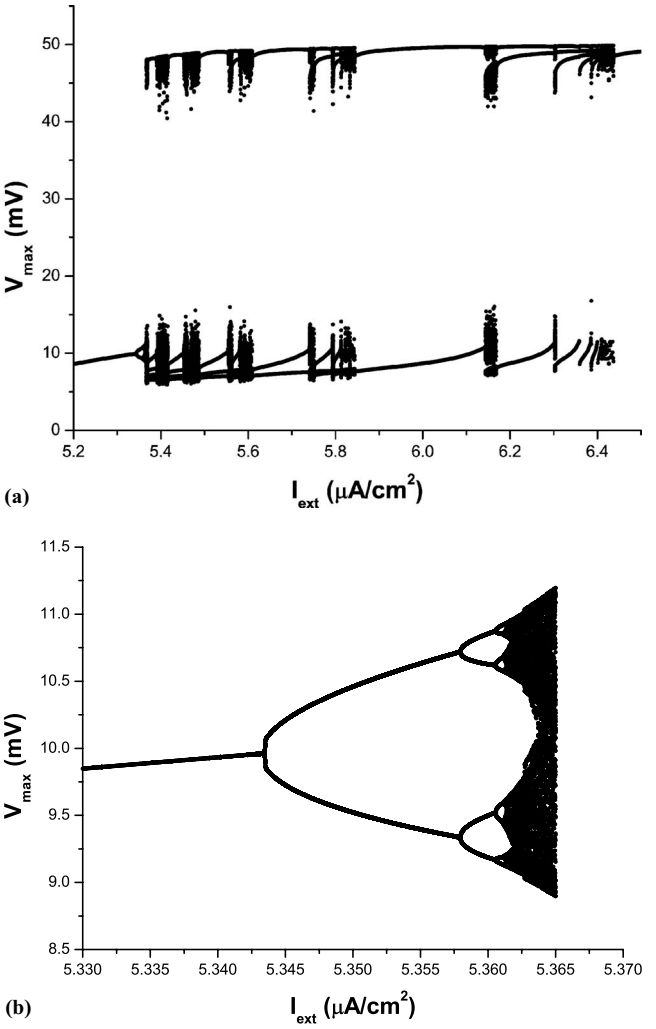

FIG. 5. (a) Bifurcation diagram of the controlled HH model with K_l=0.237 71 and K_n=−0.008 extracting local maxima of the membrane potential. (b) The enlargement of (a) in the range of I_{ext} from 5.330 to 5.365 μA/cm^2.

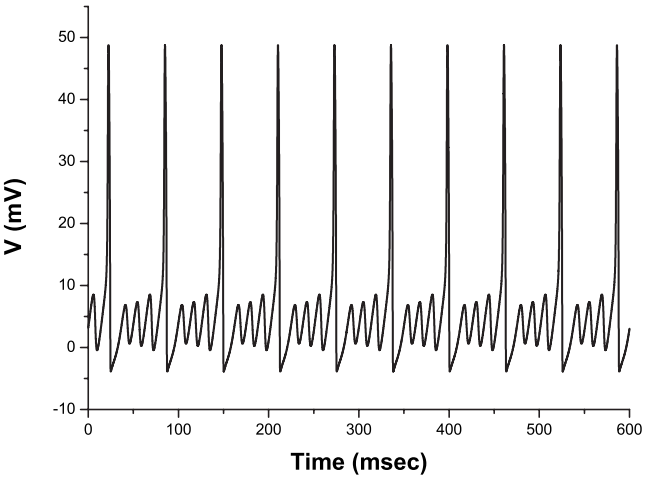

FIG. 6. Time series of the membrane potential in the controlled HH model with K_l=0.237 71, K_n=−0.008, and I_{ext}=5.5 μA/cm^2.

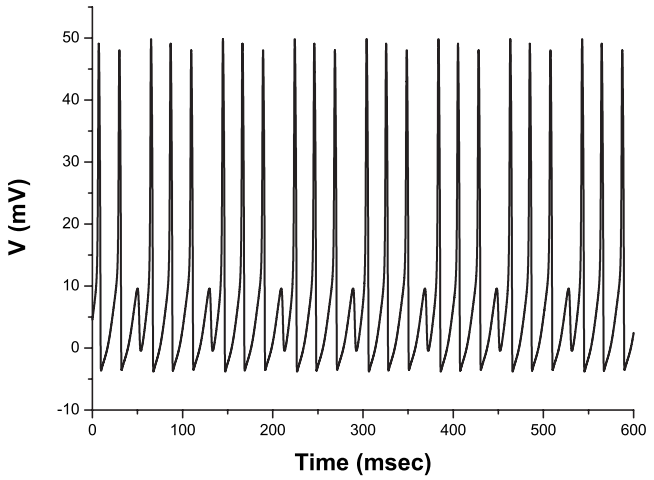

FIG. 7. Time series of the membrane potential in the controlled HH model with K_l=0.237 71, K_n=−0.008, and I_{ext}=6.33 μA/cm^2.

For instance, Fig. 8 shows the time series of the membrane potential and the projection of the system's trajectory to the V-n phase plane when I_{ext}=6.15 μA/cm^2. We can see that a chaotic spiking occurs in the controlled HH model from Fig.

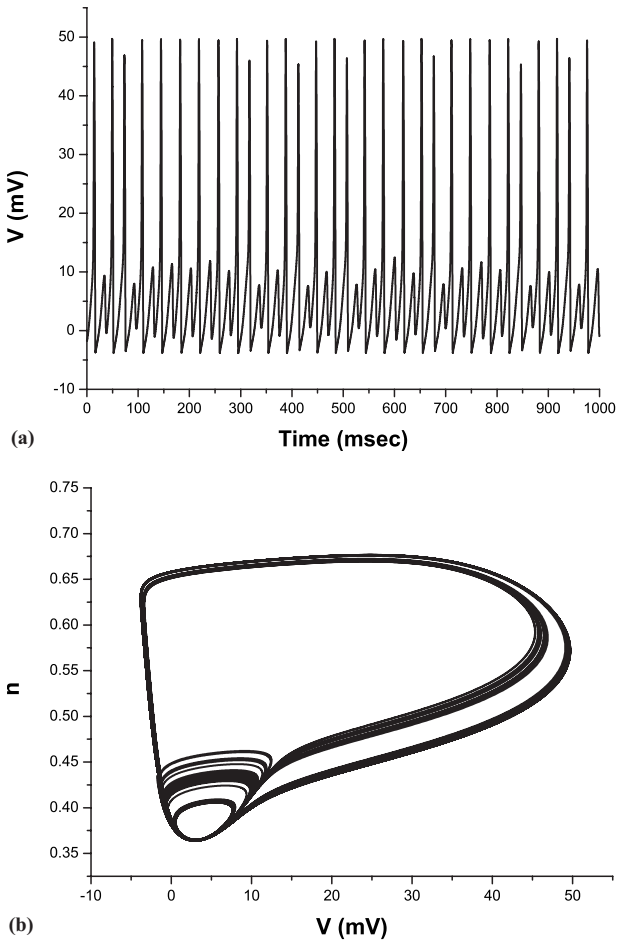

FIG. 8. (a) Time series of the membrane potential in the controlled HH model with K_l=0.237 71, K_n=−0.008, and I_{ext} =6.15 μA/cm^2. (b) The projection of the full system's trajectory to the V-n phase plane.

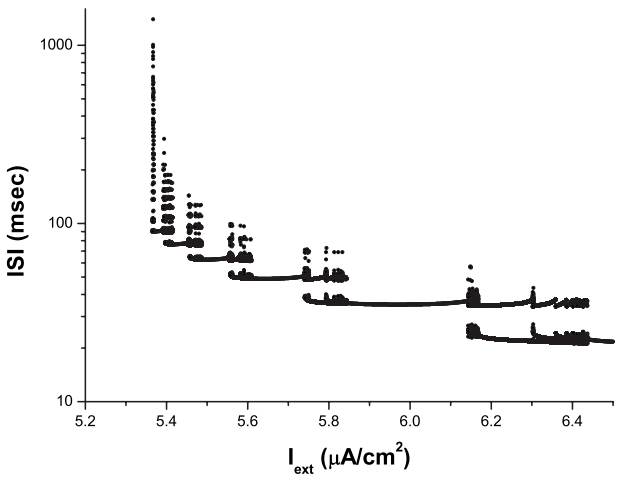

FIG. 9. Bifurcation diagram of ISI versus I_{ext} in the controlled HH model with K_l=0.237 71 and K_n=−0.008.

8. Note that this kind of chaotic spiking does not arise in the original HH model.

More interestingly, the phenomenon with slow firing appears in the controlled HH model. Figure 9 shows the change in the interspike intervals (ISIs) of the controlled HH model with K_l=0.237 71 and K_n=−0.008 as a function of I_{ext}. Note that the ordinate of Fig. 9 is the logarithm of ISIs. It is observed that the ISI increases from several tens to several thousand milliseconds as the value of I_{ext} decreases. Furthermore, the ISI becomes an arbitrary large number through more detailed numerical computations. That is, the firing rate is arbitrarily low. At about I_{ext}=5.366 μA/cm^2, the neuron terminates firing of action potentials. As we know, such slow firing in single neuron models could be achieved only by type-I neurons. Here, however the controlled HH model is still classified as a type-II neuron, as is the original HH model. It should be noted that a kind of slow firing has also been found in [35].

In what follows, we present the dynamical mechanism underlying the MMO pattern and the slow firing. Figure 10 shows the change in oscillation amplitudes as a function of I_{ext} in the controlled HH model with K_l=0.237 71 and K_n =−0.008. We can see that small-amplitude limit cycles emanate from the Hopf bifurcation at I_{ext}=5.0 μA/cm^2. At I_{ext} =5.366 μA/cm^2, the oscillation amplitude jumps abruptly from a small value to a large one. This sudden change is known as the canard explosion, witch is also called the canard phenomenon, where a small-amplitude limit cycle grows through a sequence of canard cycles to a large-amplitude relaxation oscillation as the control parameter moves through an interval of exponentially small width, and their physical implications are currently under intense investigation [36,37]. Similar to the description in [38], therefore, a transition from excitable states to spiking is found where a Hopf bifurcation is followed by a cascade of period-doubling bifurcations and chaotic small excitable attractors and, as they grow, by the canard explosion, where a small chaotic background erratically but deterministically triggers spiking in the controlled HH model. The occurrence of the MMO pattern is closely related to the canard explosion, and their

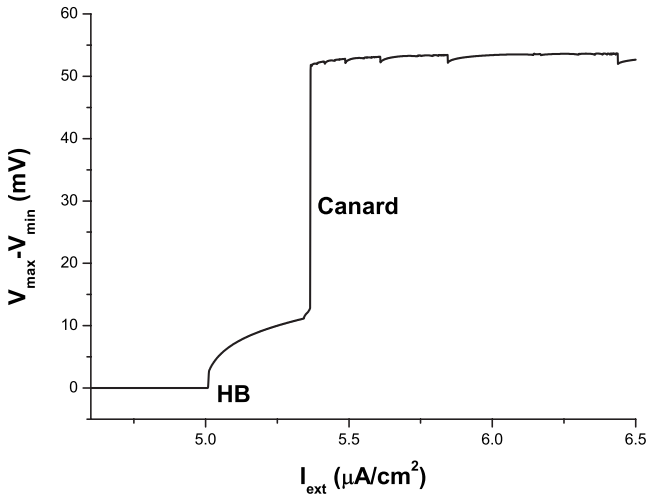

FIG. 10. Oscillation amplitudes (the maxima of the membrane potential V_{max} minus the minima of the membrane potential V_{min}) as a function of I_{ext} in the controlled HH model with K_l=0.237 71 and K_n=−0.008.

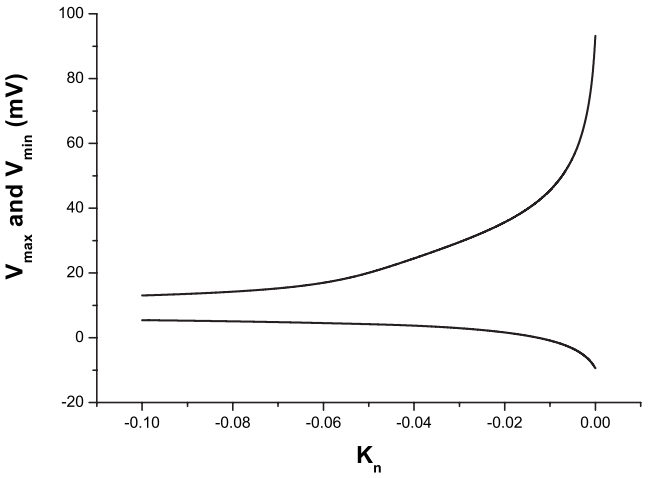

FIG. 11. The maxima and minima of the membrane potential as a function of K_n. The upper line and the lower line represent the maxima and minima of the membrane potential, respectively.

relation was first demonstrated by Milik *et al.* [33]. This type of MMO can be explained as a combination of large-amplitude relaxation oscillations and small-amplitude subthreshold oscillations mediated by canard solutions that are associated with a folded singularity on a critical manifold [33,34,39]. Canard solutions originate in a stable critical manifold and continue to an unstable critical manifold while passing through a lower fold region of nonhyperbolic behavior. In the neurodynamics canard solutions, neither perform subthreshold oscillations nor spiking, but can act as dynamic boundaries between regions of subthreshold oscillations and spiking [40]. The main difference in the dynamics between subthreshold oscillations and spiking occurs near the lower fold region of the critical manifold, where the flow of the neuronal system either jumps immediately to the upper stable critical manifold and creates a spiking or stays longer near the fold region and produces subthreshold oscillations before jumping [34]. If the unstable critical manifold is close enough to the stable critical manifold in the lower fold region, then the system's trajectory almost always moves backward toward the stable critical manifold. In this manner, such subthreshold oscillations persist over a considerably long time. Thus the period of spiking or ISI is prolonged, that is, the firing rate is slowed down.

Note that the MMOs also appear in the controlled HH model with K_l=0.237 71 and K_n=−0.007 in Fig. 4(b) (not shown).

D. Regulation of oscillation amplitude

K_n can also regulate the oscillation amplitude of the bifurcated limit cycle. In the controller, we set K_l=0.237 71 and let K_n be a free parameter. In other words, the Hopf bifurcation is advanced toward I_{ext}=5.0 μA/cm^2. Now, we calculate the maxima and minima of the membrane potential as a function of K_n at I_{ext}=20.0 μA/cm^2, as shown in Fig. 11. They correspond to the oscillation amplitudes of the bifurcated limit cycles at I_{ext}=20.0 μA/cm^2. Figure 12 illustrates the time series of the membrane potential for four different K_n values, i.e., K_n=0, −0.01, −0.03, and −0.08. From Figs. 11 and 12, it can be observed that the oscillation amplitude of the bifurcated limit cycle decreases with decreasing the value of K_n.

In this section, through a washout filter-aided dynamic feedback controller, we have successfully advanced the Hopf bifurcation toward a stable steady state according to the eigenvalue crossing condition and the transversality condition, adopting an effective measure based on the Routh-Hurwitz stability criterion. Further, the closed-form analytical expression for the bifurcation stability coefficient has been derived by the center manifold and normal form theory. We have shown the MMO pattern in the controlled HH model, presented its dynamical mechanism, and explained how a significant slowing of the firing rate may occur in this system. Finally, we have demonstrated that K_n can regulate the oscillation amplitude of the bifurcated limit cycle.

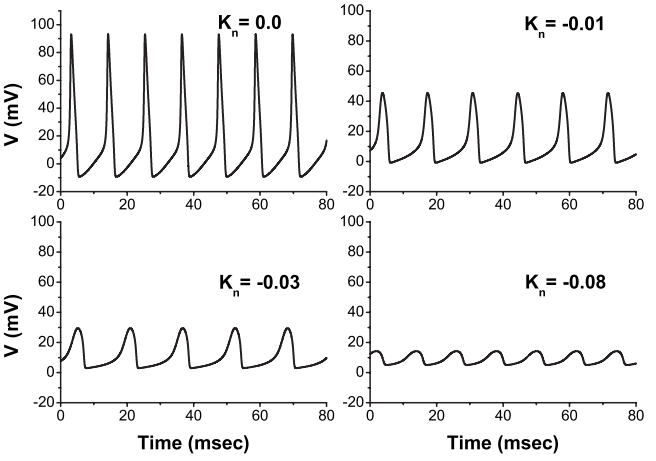

FIG. 12. Time series of the membrane potential for four different K_n values in the controlled HH model with K_l=0.237 71 and I_{ext}=20.0 μA/cm^2.

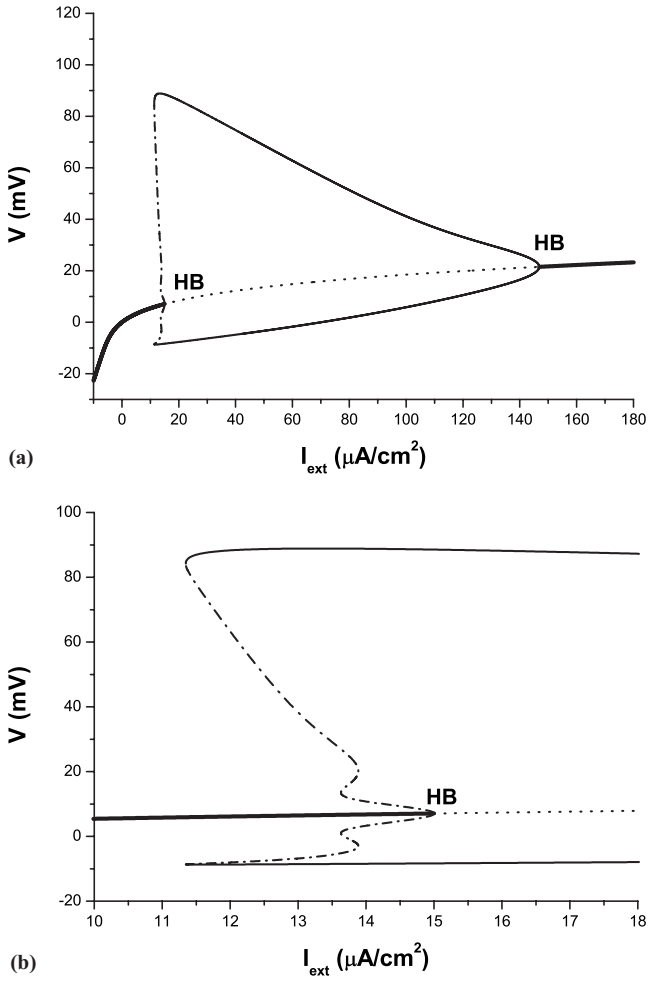

FIG. 13. (a) Bifurcation diagram of the controlled HH model with $K_l=-0.276\,81$ and $K_n=0$. (b) The enlargement of (a) near the left Hopf bifurcation point.

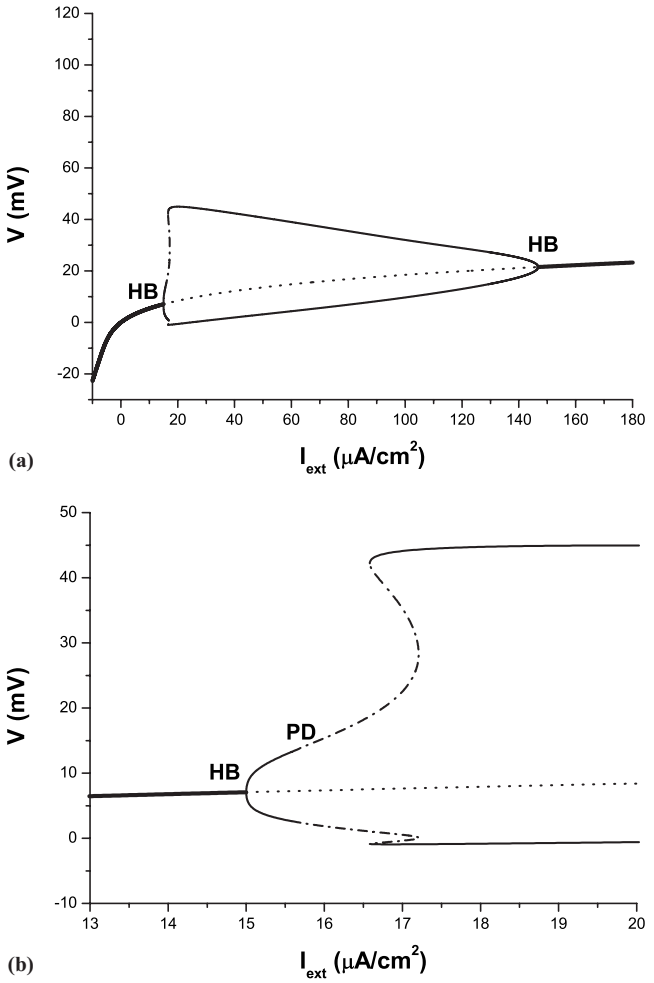

FIG. 14. (a) Bifurcation diagram of the controlled HH model with $K_l=-0.276\,81$ and $K_n=-0.0085$. (b) The enlargement of (a) near the left Hopf bifurcation point.

IV. BIFURCATION DELAY UNTIL $I_{ext}=15.0\ \mu A/cm^2$

In contrast to advancing the Hopf bifurcation toward a region of stable steady states, we can also delay the Hopf bifurcation of the original system at $I_{ext}=9.780\ \mu A/cm^2$ toward a region of unstable steady states by using the washout filter-aided dynamic feedback controller. For example, when $I_{ext}=15.0\ \mu A/cm^2$, the original system has an unstable steady state, i.e., (7.069 39, 0.117 05, 0.348 99, 0.429 26), which coexists with a stable limit cycle. In what follows, we delay the Hopf bifurcation to the bifurcation point with $I_{ext}=15.0\ \mu A/cm^2$.

In the same manner as shown in the preceding section, we can obtain $K_l=-0.276\,81$. Here, $d(\Delta_4)/dI_{ext}=-1.037\neq 0$, which satisfies the transversality condition. The bifurcation diagram of the controlled system is shown in Fig. 13. From Fig. 13(b), it is evident that the Hopf bifurcation is delayed to $I_{ext}=15.0\ \mu A/cm^2$, and it is subcritical.

Similarly, in order to control the criticality of the Hopf bifurcation, we can derive the closed-form analytical expression for the bifurcation stability coefficient as a function of K_n as follows:

$$\beta_2 = 0.106\,13\times 10^{-2} + 2\,\mathrm{Re}(0.667\,23\times 10^{-1}K_n - i0.421\,23\times 10^{-2}K_n).$$

When $K_n<-7.952\,70\times 10^{-2}$, $\beta_2<0$ and the Hopf bifurcation is supercritical. On the other hand, if $K_n>-7.952\,70\times 10^{-2}$, $\beta_2>0$ and thus the Hopf bifurcation is subcritical. We examine the change in the criticality of the bifurcation between $K_n<-7.952\,70\times 10^{-2}$ and $K_n>-7.952\,70\times 10^{-2}$. Let $K_n=-0.0085$ and -0.0075, respectively. The bifurcation diagrams for $K_n=-0.0085$ and -0.0075 are shown in Figs. 14 and 15, respectively. Obviously, with regard to the criticality of the bifurcation, the former is supercritical while the latter is subcritical. Therefore, $K_n<-7.952\,70\times 10^{-2}$ ensures that the limit cycle bifurcated from the Hopf bifurcation is asymptotically stable, and the Hopf bifurcation changes from subcritical into supercritical. At the same time, it can be seen that the bifurcation point $I_{ext}=15.0\ \mu A/cm^2$ remains constant. This again shows that the nonlinear control gain K_n has no effect on the location of the bifurcation point, but influences the criticality of the bifurcation.

As with Fig. 3, there also exist MMOs between the PD cascade and the periodic spiking in Figs. 14 and 15, respectively (not shown).

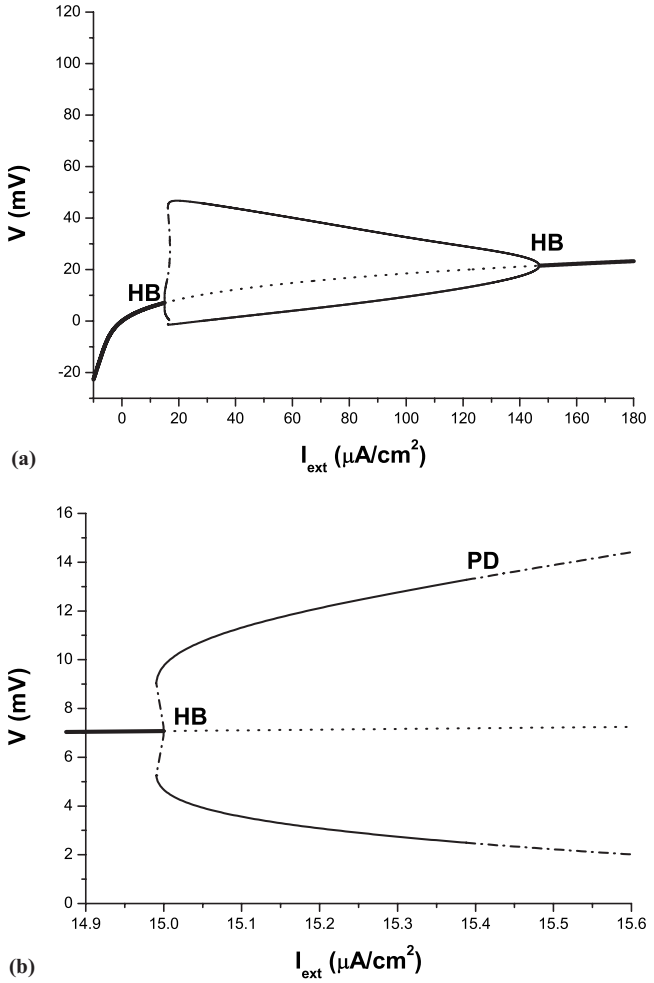

FIG. 15. (a) Bifurcation diagram of the controlled HH model with $K_l=-0.276\,81$ and $K_n=-0.0075$. (b) The enlargement of (a) near the left Hopf bifurcation point.

V. CONCLUDING REMARKS

In this study, we have controlled the onset of Hopf bifurcation in the HH model neuron. Hopf bifurcation can be moved to a desired point irrespective of whether the corresponding steady state is stable or unstable by using a washout filter-aided dynamic feedback controller. In particular, we have advanced and delayed the Hopf bifurcation to avoid its occurrence in the range from $I_{\text{ext}}=5$ to 15 $\mu\text{A}/\text{cm}^2$. The controller contains only two terms, namely the linear term and the nonlinear cubic term. We have deduced the linear control gain K_l according to the two basic critical conditions for Hopf bifurcations, i.e., the eigenvalue crossing condition and the transversality condition, by an effective measure based on the Routh-Hurwitz stability criterion. Through a coordinate transformation, the controlled HH model has been transformed into a new system with a canonical form. Thus, the closed-form analytical expression for the bifurcation stability coefficient, which is a function of the nonlinear control gain K_n, has been derived by the application of the center manifold and normal form theory. In this manner, we can change the criticality of the Hopf bifurcation from subcritical to supercritical by the nonlinear control gain K_n. It has been observed that the nonlinear control gain K_n has no effect on the location of the bifurcation. We have also shown that the MMO pattern occurs in the controlled HH model, presented that it is closely related to the canard explosion, and explained how a significant slowing of the firing rate may occur in this system. Moreover, we have shown that chaotic spiking appears in the controlled HH model. Note that the MMO pattern and chaotic spiking do not occur in the original HH model. Finally, we have shown that K_n can regulate the oscillation amplitude of the limit cycle bifurcated from the Hopf bifurcation. By controlling the onset of Hopf bifurcation in the HH model neuron, we believe that the information provided in this paper may have important implications for the understanding of the underlying physiological mechanisms, and may establish a possible starting point for future clinical applications for dynamical diseases of the nervous system.

ACKNOWLEDGMENTS

This work was partially supported by the National Natural Science Foundation of China under Grants No. 10502039, No. 10602041, and No. 10432010 and a Grant-in-Aid for Scientific Research on Priority Areas—System study on higher-order brain functions—from MEXT of Japan (17022012). Y.X. is grateful to the MEXT of Japan for financial support.

[1] M. C. Mackey and U. An Der Heiden, Func. Biol. Med. **154**, 156 (1982).
[2] L. Glass and M. C. Mackey, *From Clocks to Chaos: The Rhythms of Life* (Princeton University Press, Princeton, NJ, 1988).
[3] J. Belair, L. Glass, U. An Der Heiden, and J. Milton, Chaos **5**, 1 (1995).
[4] P. E. Rapp, R. A. Latta, and A. I. Mees, Bull. Math. Biol. **50**, 227 (1988).
[5] M. C. Mackey and J. G. Milton, Ann. N.Y. Acad. Sci. **504**, 16 (1987).
[6] F. H. Lopes da Silva and J. P. M. Pijn, Adv. Neurol. **81**, 97 (1999).
[7] U. an der Heiden, Pharmacopsychiatry **39**, S36 (2006).
[8] J. Milton and P. Jung, *Epilepsy as a Dynamic Disease* (Springer-Verlag, New York, 2002).
[9] http://www.dchaos.com/portfolio/dchaos1/new_nonlinear_man_article.html
[10] L. Pujo-Menjouet and M. C. Mackey, C. R. Biologies **327**, 235 (2004).
[11] G. Chen, J. L. Moiola, and H. O. Wang, Int. J. Bifurcation Chaos Appl. Sci. Eng. **10**, 511 (2000).

[12] H. O. Wang and E. H. Abed, Automatica **31**, 1213 (1995).
[13] E. H. Abed and J. H. Fu, Syst. Control Lett. **7**, 11 (1986).
[14] E. H. Abed, H. O. Wang, and R. C. Chen, Physica D **70**, 154 (1994).
[15] D. W. Berns, J. L. Moiola, and G. Chen, Automatica **34**, 1567 (1998).
[16] W. Kang, SIAM J. Control Optim. **36**, 193 (1998).
[17] M. A. Kramer, B. A. Lopour, H. E. Kirsch, and A. J. Szeri, Phys. Rev. E **73**, 041928 (2006).
[18] H. C. Lee and E. H. Abed, In *Proceedings of the American Control Conference, Boston, 1991* (American Automatic Control Council, Green Valley, AZ, 1991), pp. 206–211.
[19] Y. Xie, K. Aihara, and Y. M. Kang, Phys. Rev. E **77**, 021917 (2008).
[20] S. Tsuji, T. Ueta, H. Kawakami, H. Fujii, and K. Aihara, Int. J. Bifurcation Chaos Appl. Sci. Eng. **17**, 985 (2007).
[21] A. L. Hodgkin and A. F. Huxley, J. Physiol. (London) **117**, 500 (1952).
[22] J. Wang, L. Q. Chen, and X. Y. Fei, Chaos, Solitons Fractals **33**, 217 (2007).
[23] J. Guckenheimer and P. Holmes, *Nonlinear Oscillations, Dynamical Systems, and Bifurcations of Vector Fields*, 5th ed. (Springer, New York, 1997), pp. 150–152.
[24] D. S. Chen, H. O. Wang, and G. Chen, IEEE Trans. Circuits Syst., I: Fundam. Theory Appl. **48**, 661 (2001).
[25] K. Aihara and G. Matsumoto, J. Theor. Biol. **95**, 697 (1982).
[26] B. Ermentrout, *Simulating, Analyzing, and Animating Dynamical Systems: A Guide to XPPAUT for Researchers and Students* (SIAM, Philadelphia, 2002).
[27] E. Doedel, H. B. Keller, and J. P. Kernevez, Int. J. Bifurcation Chaos Appl. Sci. Eng. **1**, 493 (1991).
[28] M. A. Hassouneh, H. C. Lee, and E. H. Abed, in *Proceeding of the 2004 American Control Conference, Boston* (IEEE, New York, 2004), pp. 3950–3955.
[29] G. L. Wen and D. L. Xu, Phys. Lett. A **337**, 93 (2005).
[30] W. M. Liu, J. Math. Anal. Appl. **182**, 250 (1994).
[31] B. D. Hassard, N. D. Kazarinoff, and Y. H. Wan, *Theory and Application of Hopf Bifurcation*, London Mathematical Society Lecture Note Series Vol. 41 (Cambridge University Press, Cambridge, 1981), pp. 86–91.
[32] V. Petrov, S. K. Scott, and K. Showalter, J. Chem. Phys. **97**, 6191 (1992).
[33] A. Milik, P. Szmolyan, H. Loeffelmann, and E. Groeller, Int. J. Bifurcation Chaos Appl. Sci. Eng. **8**, 505 (1998).
[34] J. Rubin and M. Wechselberger, Biol. Cybern. **97**, 5 (2007).
[35] S. Doi and S. Kumagai, J. Comput. Neurosci. **19**, 325 (2005).
[36] E. I. Volkov, E. Ullner, A. A. Zaikin, and J. Kurths, Phys. Rev. E **68**, 026214 (2003).
[37] X. M. Li, J. Wang, and W. H. Hu, Phys. Rev. E **76**, 041902 (2007).
[38] F. Marino, F. Marin, S. Balle, and O. Piro, Phys. Rev. Lett. **98**, 074104 (2007).
[39] M. Brøns, M. Krupa, and M. Wechselberger, Fields Inst. Commun. **49**, 39 (2006).
[40] J. Moehlis, J. Nonlinear Sci. **12**, 319 (2002).